

CALCULATION OF ROTOR BLADE-VORTEX INTERACTION NOISE USING PARALLEL SUPER COMPUTER

Takashi AOYAMA,

National Aerospace Laboratory

7-44-1, Jindaijihigashi-machi, Chofu, Tokyo 182, Japan

Natsuki KONDO, Makoto AOKI, Hideaki NAKAMURA,
Advanced Technology Institute of Commuter-helicopter, Ltd.
2 Kawasaki-cho, Kagamigahara City, Gifu-Pref. 504, Japan

Shigeru SAITO

National Aerospace Laboratory

7-44-1, Jindaijihigashi-machi, Chofu, Tokyo 182, Japan

Abstract

A prediction method for blade-vortex interaction (BVI) noise of a helicopter rotor is developed. This method consists of following four steps: 1) trim analysis using CAMRAD II based on a lifting-line theory, 2) interpolation of the blade motion and the wake geometry, 3) aerodynamic analysis using a finite difference solver for the three-dimensional unsteady Euler equations, and 4) noise analysis using an aeroacoustic code based on the Ffowcs Williams and Hawkings (FW-H) formulation without the quadrupole term. The predicted acoustic waveform for the OLS model rotor is compared with experimental data and reasonable correlation is obtained. This method is applied to investigate the effect of the tip shape on the intensity of the BVI noise. For the first step, the effects of anhedral, dihedral, tapered, and swept tip shapes are discussed. The most time-consuming step of our prediction method is the unsteady Euler calculation. In this study, the calculation is performed using Numerical Wind Tunnel (NWT) in National Aerospace Laboratory (NAL). The NWT is a parallel super computer which consists of 166 processing elements (PEs). The total peak performance of the NWT is about 280GFLOPS and the total capacity of the main memory is as much as 45GB. The NWT makes it possible to conduct our parametric study for the effect of the blade-tip shape on the intensity of the BVI noise.

Introduction

Main rotor of a helicopter generates two types of impulsive noise. One is the high-speed impulsive (HSI) noise which is caused by the shock wave generated on the blade surface of the advancing side in

high-speed forward flight. The other is the blade-vortex interaction (BVI) noise which is caused by the sudden change of the blade loads during the interactions of the blade with previously shed tip vortices. Ref.[1] helps us to understand the mechanism of the occurrence of the BVI noise. In general, the interactions occur in descent flight conditions, especially during approach to a landing. The noise generated by the interactions radiates mostly below the helicopter's tip-path plane in the direction of forward flight. The acoustic signal is generally in the frequency range most sensitive to human subjective response (500 to 5000Hz) [2]. The BVI noise, therefore, prevents that the commuter helicopter is widely used in the densely populated area. In 1994, Advanced Technology Institute of Commuter-helicopter (ATIC) is established in Japan in order to investigate the noise and safety problems of helicopters. This paper reports the results of the collaborative research between National Aerospace Laboratory (NAL) and ATIC. The main objectives of the collaborative research are to develop prediction methods of rotor noise and to investigate reduction methods for the noise.

Many efforts have been made in both experimental and theoretical researches about the BVI noise. Ref.[3] presents a review of the recent researches about the BVI aerodynamics. It covers both analytical and experimental studies of two-dimensional parallel airfoil-vortex interactions, three-dimensional BVIs and helicopter rotor BVIs. A procedure was developed for the prediction of the BVI noise by coupling a lifting-line model, a three-dimensional unsteady full potential solver, and a linearized acoustic formulation [4]. It is reported that several methods which couple aerodynamic and aeroacoustic codes have been developed to predict the BVI noise by the Aeroflight-dynamics Directorate (AFDD) of the U.S. Army, DLR of Germany,

and ONERA of France, respectively [5]. One of the two objectives of this study is to develop a prediction method of the BVI noise. A method which couples a trim code, an aerodynamic code, and an aeroacoustic code is developed.

The intensity of the BVI noise is strongly affected by the factors, 1) the local strength of the tip vortex, 2) the core size of the tip vortex, 3) the local interaction angle between the blade and the vortex line, and 4) the miss-distance between the vortex and the blade [1]. It is known that some kinds of tip shapes may reduce the intensity of the BVI noise. Time histories of the BVI noise were measured by using an in-flight technique for the UH-1H helicopter with its standard NACA0012 airfoil rotor and the AH-1S helicopter configured with its standard 540 rotor, the Kaman K747 rotor, and the OGEE tip rotor [6]. A cooperative research was performed between AFDD, the NASA Ames and Langley Research Centers, the United Technologies Research Center (UTRC), and the Sikorsky Aircraft Division of United Technologies in order to improve understanding of rotor aerodynamics, acoustics, and dynamics including the effect of blade-tip shape [7]. An experimental research was conducted in order to characterize the BVI noise created by various blade geometries as a function of rotor operating parameters [2]. The tip-vortex structure of several tip shapes were examined experimentally in non-rotational conditions to investigate tip shapes for reduced BVI [8][9]. However, the comprehensive understanding of the effect of the tip shape on the intensity of the BVI noise has not been obtained yet. Therefore, the second objective of this study is to investigate its effect. For the first step, the effects of anhedral, dihedral, swept, and tapered tip shapes are discussed. The anhedral and dihedral tip shapes are selected in order to investigate the effect of the miss-distance between the vortex and the blade on the intensity of the BVI noise. The swept and tapered tip shapes are also selected in order to investigate the effect of the local interaction angle between the blade and the vortex line and the effect of the local strength and the core size of the tip vortex on the intensity of the BVI noise, respectively.

The most time-consuming step of our prediction method is the unsteady Euler calculation. In this study, the calculation is performed using Numerical Wind Tunnel (NWT) in NAL. The NWT is a parallel super computer which consists of 166 processing elements (PEs). The performance of an individual PE is equivalent to that of a super computer, 1.7GFLOPS. Each PE has a main memory of 256MB. High-speed cross-bar network connects 166PEs. The total peak performance of the NWT is about 280GFLOPS and the total capacity of the main memory is as much as 45GB. In the case of our calculation to predict the BVI noise, the typical dividing number along the azimuthal direction

is about 2000/rev. It takes less than 1 hour to obtain a fully converged solution for about 150,000 grid points by using 36 PEs. The NWT makes it possible to conduct our parametric study for the effect of the blade-tip shape on the intensity of the BVI noise.

Calculation Method

The method used in this study consists of following four steps as shown in Fig.1: 1) trim analysis using CAMRAD II based on a lifting-line theory, 2) interpolation of the blade motion and the wake geometry, 3) aerodynamic analysis using a finite difference solver [10] for the three-dimensional unsteady Euler equations, and 4) noise analysis using an aeroacoustic code [11] based on the Ffowcs Williams and Hawkings (FW-H) formulation.

In the first step, the blade motion and the wake geometry are obtained as the result of the free-wake analysis of CAMRAD II owned by ATIC. The code is run in 10-deg azimuthal increments. However, it is too coarse to capture the instantaneous BVI events. Therefore, the azimuthal resolution is improved to 1 deg in the second step by using the method similar to that in ref.[12]. The core radius is a user specified parameter in CAMRAD II. It is set $0.3C$ except for the tapered blade case in which it is set $0.5C$ for the blade with the taper ratio of 0.3 according to ref.[8]. The quantity C is the chord length of the blade here.

In the third step, the governing equations are the three-dimensional unsteady Euler equations in the blade fixed rotating Cartesian coordinate system. In order to conduct the calculation with arbitrary curved grid, these equations are transformed from the Cartesian coordinate system to the arbitrary curvilinear coordinate system. The numerical method to solve the governing equations is an implicit finite-difference scheme. A higher-order upwind scheme based on TVD is applied for the inviscid terms of the explicit right-hand side. To obtain the unsteady solution in the forward flight condition of a helicopter rotor, the Newton iterative method is added. In the beginning of the calculation, the steady calculation is conducted at $\psi = 90^\circ$ using the implicit time-marching method. Then, the unsteady calculation is started from this initial condition. Periodic converged solutions are obtained at about $\psi = 360^\circ$. Four iterations are sufficient to reduce the residual at each time step. The effect of the wake is modeled by using the angle-of-attack approach in which the effect of the disturbance caused by the blade-vortex interaction is only felt through the surface boundary condition. The effective angle of attack obtained in the second step is used in this boundary condition.

In the fourth step, the aeroacoustic code utilizes the FW-H formulation without the quadrupole term

because strong shock waves are not generated in the flight condition considered here. The acoustic pressure at an observer position is calculated by using the pressure distributions on the blade surface obtained in the third step.

Results and Discussions

In this section, the comparison between measured and calculated time histories of the BVI noise is shown first. Then, the effects of anhedral, dihedral, swept, and tapered tip shapes on the intensity of the BVI noise are discussed.

Comparison between measured and calculated results

Calculations are performed to predict the BVI noise of the 1/7-scale model AH-1 Operational Loads Survey (OLS) blades obtained in the German-Dutch Wind Tunnel (DNW) [13]. The blade geometry and the condition are shown in Table 1 and Table 2, respectively. The observer position is shown in Fig.2. The quantity R is the rotor radius in this figure. The predicted acoustic waveform for the OLS model rotor is compared with experimental data obtained by Spletstoeser et al.[13] in Fig.3. Two positive peaks of the sound pressure, A and B, are observed both in the measured and calculated time histories. Therefore, the calculated result adequately predicts the number of the BVI events. The amplitude of the peak A is underpredicted but that of the peak B is accurately predicted. A top view of the predicted BVI location is shown in Fig.4. The open and filled circle respectively represent the interaction above and below the rotor disk. The miss-distance is indicated by the size of the circle. The larger circle means the close interaction. The BVI noise is usually radiated from the outer 20-30 % of the blade in the advancing side. In Fig.4, the interactions A and B indicate the interactions between the outer blade and the vortex in the advancing side. Each interaction causes the peak A and B in Fig.3, respectively. Figure 5 shows the miss-distance between the vortex and the blade during the blade-vortex interactions. The quantity dz is the vertical distance between the vortex and the blade. The open and filled circle respectively represent the interaction of the blade with the vortex shed from the own blade and the vortex shed from the previous blade. The interactions A and B in Fig.5 correspond to the interactions A and B in Fig.4, respectively. According to the time history in Fig.3(a) the miss-distance of the interaction A should be smaller than that of the interaction B. However, the miss-distance of the interaction A is larger than that of the interaction B in Fig.5. It seems that the underprediction for the peak A is caused by the reason why the miss-distance between the blade and the vortex shed from

the own blade, which travels longer than the vortex shed from the previous blade before the blade-vortex interaction, is not so accurate in the first step of our prediction method. Our additional calculation confirms that to artificially reduce the miss-distance of the interaction A makes a larger amplitude of the peak A as mentioned in ref.[4].

Effect of Anhedral and Dihedral

The anhedral and dihedral tip shapes are selected in order to investigate the effect of the miss-distance between the vortex and the blade on the intensity of the BVI noise. Figure 6 shows the time histories of the BVI noise for the blades with anhedral, rectangular, and dihedral tip shapes. Both the anhedral and dihedral angles are 20° as illustrated in Figs.6(a) and (c). The modifications start from $0.9R$ radial station as also illustrated in Figs.6(a) and (c). Figure 7 shows the strength of the tip vortex during the blade-vortex interactions for the blades with anhedral, rectangular, and dihedral tip shapes. The quantity Γ is the tip-vortex circulation and V_{tip} is the rotor rotational speed at the tip. The open and filled circle respectively represent the interaction of the blade with the vortex shed from the own blade and the vortex shed from the previous blade. It is observed that the strength is almost same among the three types of the tip shapes. Figure 8 shows the miss-distance between the vortex and the blade during the blade-vortex interactions for the blades with anhedral, rectangular, and dihedral tip shapes. The miss-distances of the interaction A and B are larger in Fig.8(a) than in Fig.8(b). Therefore, the amplitudes of the peak A and B are smaller in Fig.6(a) than in Fig.6(b). The miss-distance of the interaction A is smaller in Fig.8(c) than in Fig.8(b) and the miss-distance of the interaction B is larger in Fig.8(c) than in Fig.8(b). Therefore, the amplitude of the peak A is larger in Fig.6(c) than in Fig.6(b) and the amplitude of the peak B is smaller in Fig.6(c) than in Fig.6(b). It is concluded that in this case the anhedral tip shape decreases the BVI noise because it increases both the miss-distances of the interaction A and B. It is also concluded that in this case the dihedral tip shape doesn't always increase the BVI noise because it decreases the miss-distance of the interaction A but increases that of the interaction B. Much more calculations are needed to obtain the comprehensive understanding of the effect of the anhedral and dihedral tip shapes.

Effect of Sweep

The swept tip shapes are selected in order to investigate the effect of the local interaction angle between the blade and the vortex line on the intensity of the BVI noise. Figure 9 shows the time histories of the BVI noise for the blades with swept-forward, rectangular, and swept-back tip shapes.

Both the sweepback and sweepforward angles are 40° as illustrated in Figs.9(a) and (c). The modifications start from $0.9R$ radial station as also illustrated in Figs.9(a) and (c). Figure 10 shows the strength of the tip vortex during the blade-vortex interactions for the blades with swept-forward, rectangular, and swept-back tip shapes. It is observed that the strength is almost same among the three types of the tip shapes. Figure 11 shows the miss-distance between the vortex and the blade during the blade-vortex interactions for the blades with swept-forward, rectangular, and swept-back tip shapes. The miss-distance is not so different among the three types of the tip shapes. Figure 12 shows the calculated trajectories of the tip vortex for the blades with swept-forward, rectangular, and swept-back tip shapes. The azimuth angles of the blade location are 72° and 252° in Figs.12(a), (b), and (c). In the tip region of the advancing side, the local interaction angle between blade and vortex line is different among the three types of the tip shapes. The angle is nearly 90° in the case of the swept-forward tip shape. This type of perpendicular interaction doesn't cause strong BVI noise. Therefore, the amplitudes of the peak A and B are much smaller in Fig.9(a) than in Fig.9(b). On the other hand, the angle is almost 0° in the case of the swept-back tip shape. This type of parallel interaction generates strong BVI noise. It doesn't seem that the result of the interaction angle is reflected in the amplitude of the peak A in Fig.9(c). The reason is shown in Fig.13. In this figure, the effect of swept tip shapes on the directivity of the BVI noise is indicated. Figures 13(a)-(c), (d)-(f), and (g)-(i) respectively show the results at the observer positions 2, 1, and 3 as illustrated in Fig.13. In comparison of Figs.13(b), (e), and (h), the intensity of the BVI noise is strongest at the observer position 1. However, in comparison of Figs.13(c), (f), and (i), the intensity is strongest at the observer position 2. The directivity of the radiation, therefore, is shifted toward the right hand side of the forward flight direction by the swept-back tip shape. The amplitudes of the peak A and B in Fig.13(c) are much larger than those in Fig.13(e) because the local interaction angle between the blade and the vortex line is almost 0° in the swept-back tip region. Such kind of shift in the directivity is not clear in the case of swept-forward tip shape because the strong interaction doesn't occur in the swept region. It is concluded that in this case the blade with the swept-forward tip shape reduces the BVI noise because it causes the perpendicular BVI in the tip region in the advancing side. On the other hand, the blade with the swept-back tip shape intensifies the BVI noise because it causes the parallel BVI in the tip region in the advancing side. The directivity of the radiation shifts toward the right hand side of the forward flight direction in the case of the swept-back

tip shape.

Effect of Taper

The tapered tip shape is selected in order to investigate the effect of the the local strength and the core size of the tip vortex on the intensity of the BVI noise. Figure 14 shows the time histories of the BVI noise for the blades with tapered and rectangular tip shapes. The taper ratio is 0.3 as illustrated in Fig.14(a). The modification starts from $0.9R$ radial station as also illustrated in Fig.14(a). It is observed that the amplitudes of A and B are reduced by the tapered tip shape. Figure 15 shows the strength of the tip vortex during the blade-vortex interactions for the blades with tapered and rectangular tip shapes. The strength is almost same between the two types of the tip shapes. Figure 16 shows the miss-distance between the vortex and the blade during the blade-vortex interactions for the blades with tapered and rectangular tip shapes. The miss-distance is not so different between the two types of the tip shapes. The core radius of the tip vortex is a user specified parameter in the first step of our calculation method. The effect of tapered tip shape on the core radius is not so clear at present. In this research, a larger core radius is used for the tapered tip shape than for the rectangular one. The core radii for the blades with tapered and rectangular tip shapes are $0.5C$ and $0.3C$, respectively. Figure 17 shows the time histories of the effective angle of attack for the rectangular and tapered tip shapes. The calculated effective angle of attack is directly affected by the core radius. The amplitudes of the peak in the advancing and retreating side are remarkably reduced by the tapered tip shape compared with the rectangular one. The effective angle of attack has a strong correlation with the blade load. Therefore, it is concluded that the intensity of the BVI noise is reduced by the tapered tip shape for which a core radius larger than that for the rectangular tip shape is applied. More detailed experimental result about the strength and the core size of the tip vortex is needed to obtain the comprehensive understanding of the effect of the tapered tip shape.

Conclusions

A calculation method which couples a trim code, an aerodynamic code, and an aeroacoustic code is applied to predict the BVI noise of the OLS model rotor. The following conclusion is obtained.

- The calculated result adequately predicts the number of the BVI events. The amplitude of the peak A is underpredicted but that of the peak B is accurately predicted.

The calculation method is applied to investigate the effect of the tip shape on the intensity of the BVI noise. For the first step, the effects of anhedral, dihedral, tapered, and swept tip shapes are discussed. The following major conclusions are obtained.

- The anhedral tip shape decreases the BVI noise because it increases both the miss-distances of the interaction A and B. The dihedral tip shape doesn't always increase the BVI noise because it decreases the miss-distance of the interaction A but increases that of the interaction B.
- The swept-forward tip shape reduces the BVI noise because it causes the perpendicular BVI in the tip region in the advancing side. On the other hand, the swept-back tip intensifies the BVI noise because it causes the parallel BVI in the tip region in the advancing side. The directivity of the radiation shifts toward the right hand side of the forward flight direction in the case of the swept-back tip shape.
- The intensity of the BVI noise is reduced by the tapered tip shape for which a core radius larger than that for the rectangular tip shape is applied.

References

1. Schmitz, F.H. and Yu, Y.H., Helicopter Impulsive Noise: Theoretical and Experimental Status, *Journal of Sound and Vibration*, 109(3), 1986, pp.361-422.
2. Martin, R.M. and Connor, A.B., Wind-Tunnel Acoustic Results of Two Rotor Models with Several Designs, NASA-TM 87698, 1986.
3. Tung, C., Yu, Y.H., and Low, S.L., Aerodynamic Aspects of Blade-Vortex Interaction (BVI), AIAA Paper 96-2010, June 1996.
4. Tadghighi, H., Hassan, A.A., and Charles, B., Prediction of Blade-Vortex Interaction Noise Using Airloads Generated by a Finite-Difference Technique, *Journal of the American Helicopter Society*, Vol.37, No.4, October 1992, pp.38-47.
5. Yu, Y.H., Tung, C., Gallman, J., Klaus, K.J., Van der Wall, B., Spiegel, P., and Michea, B., Aerodynamics and Acoustics of Rotor Blade-Vortex Interactions, *Journal of Aircraft*, Vol.32, No.5, Sep.-Oct. 1995, pp.970-977.
6. Boxwell, D.A. and Schmitz, F.H., Full-Scale Measurements of Blade-Vortex Interaction Noise, *Journal of the American Helicopter Society*, Vol.27, (4), October 1982, pp.11-27.
7. Yu, Y.H., Liu, S.R., Jordan, D.E., Landgrebe, A.J., Lorber, P.F., Pollack, M.J., and Martin, R.M., Aerodynamic and Acoustic Test of a United Technologies Model Scale Rotor at DNW, 46th Annual Forum of the American Helicopter Society, May 1990.
8. Wagner, W.J., Comparative Measurements of the Unsteady Pressures and the Tip-Vortex Parameters on four Oscillating Wing Tip Models, 10th European Rotorcraft Forum, Nr.9, August 1984.
9. Mullins, B.R. Jr, Smith, D.E., Rath, C.B., and Thomas, S.L., Helicopter Rotor Tip Shapes for Reduced Blade-Vortex Interaction - An Experimental Investigation, Part II, AIAA Paper 96-0149, 1996.
10. Aoyama, T., Kawachi, K., and Saito, S., Effect of Blade-Tip Planform on Shock Wave of Advancing Helicopter Blade, *Journal of Aircraft*, Vol.32, No.5, Sep.-Oct. 1995, pp.955-961.
11. Nakamura, Y. and Azuma, A., Rotational Noise of Helicopter Rotors, *Vertica*, vol.3, no.3/4, 1979, pp.293-316.
12. Hassan, A.A., Tung, C., and Sankar, L.N., An Assessment of Full Potential and Euler Solutions for Self-Generated Rotor Blade-Vortex Interactions, 46th Annual Forum of the American Helicopter Society, May 1990.
13. Spletstoesser, W.R., Schultz, K.J., Boxwell, D.A., and Schmitz, F.H., Helicopter Model Rotor Blade Vortex Interaction Impulsive Noise: Scalability and Parametric Variations, 10th European Rotorcraft Forum, Paper Nr.18, 1984.

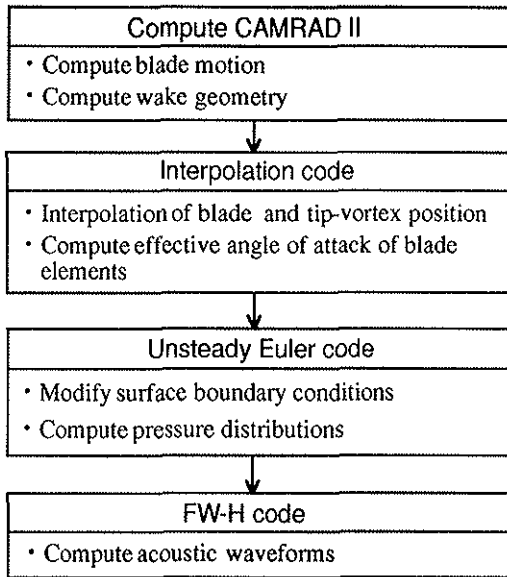


Fig.1 Flow chart illustrating the calculation method.

Table 1 Main rotor characteristics.

AH-1/OLS model rotor	
Radius	0.958 m
Chord length	0.104 m
Solidity	0.056
Number of blade	2
Airfoil	modified BHT 540 (t/c = 9.71 %)
Hinge	teeter type
Tip planform	rectangular

Table 2 Operating condition.

Hover tip Mach number	0.664
Forward speed	72.0 kts
Advance ratio	0.164
Rotor thrust coefficient	0.0054
Shaft inclination angle	2.0 deg (+ aft.)

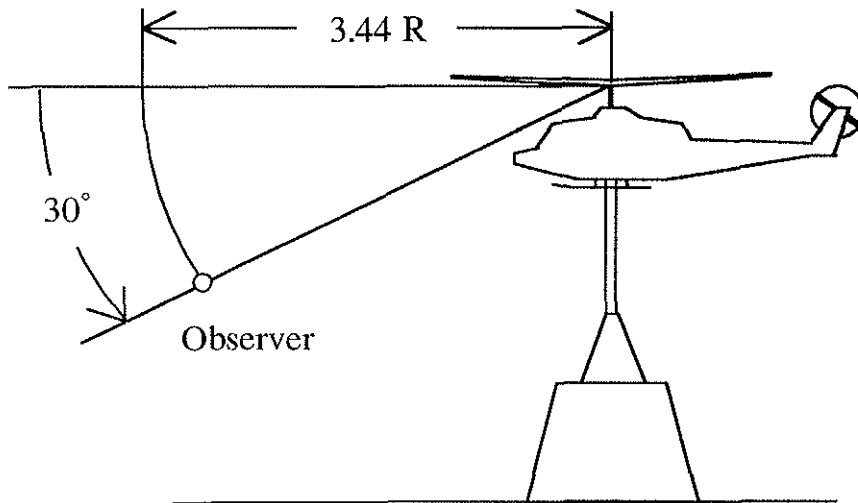


Fig.2 Observer position.

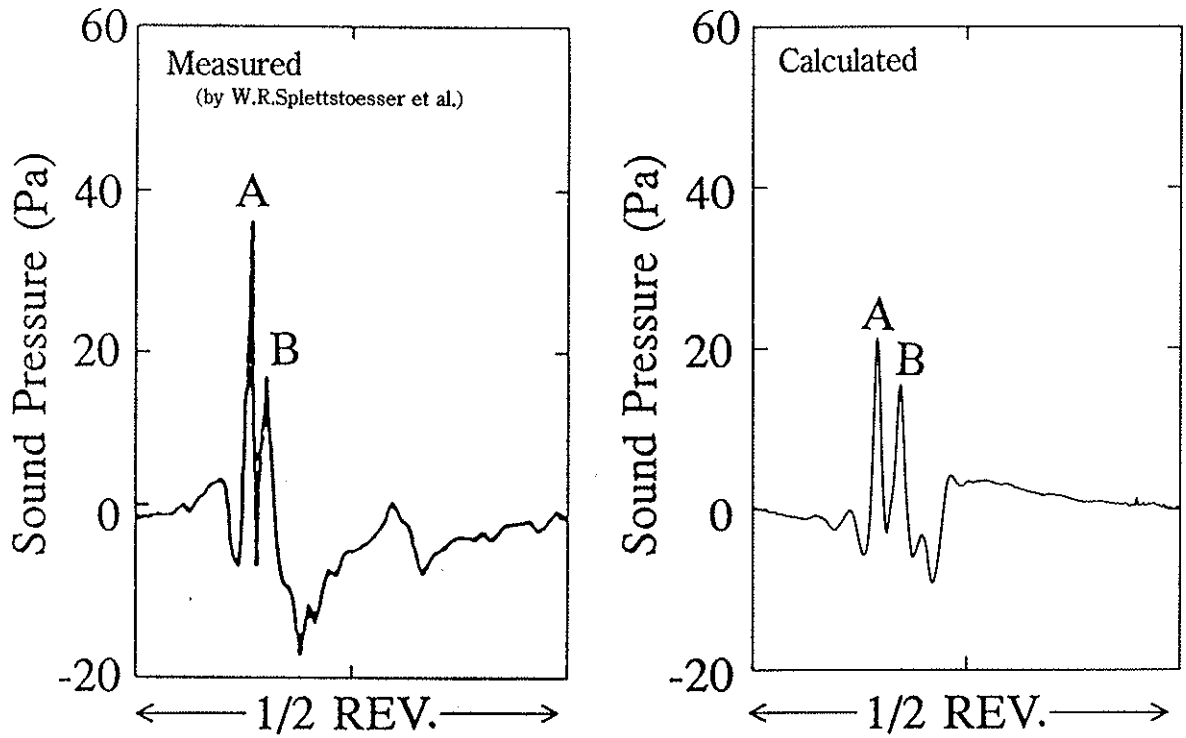


Fig.3 Comparison between measured and calculated time histories of BVI noise.

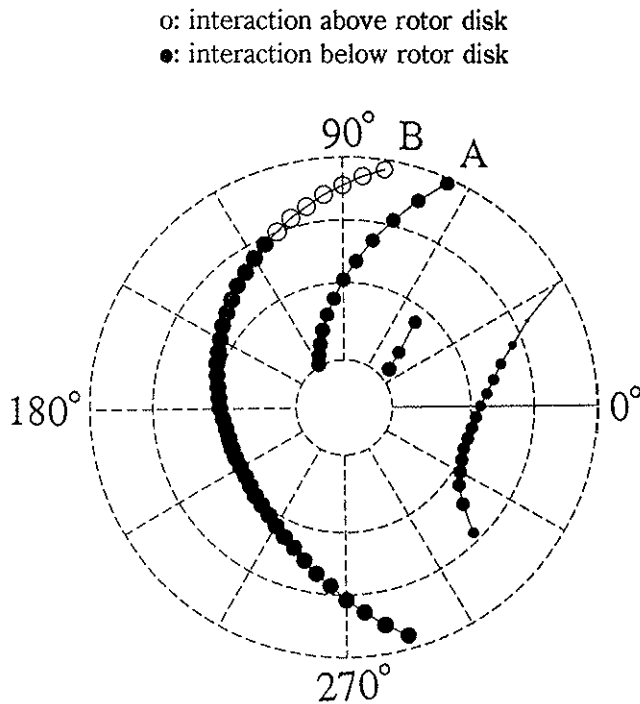


Fig.4 Top view of predicted BVI locations.

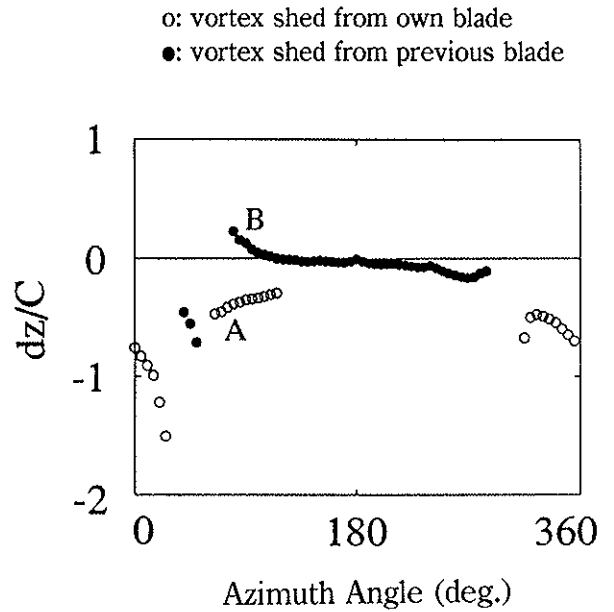


Fig.5 Miss-distance between vortex and blade during BVIs.

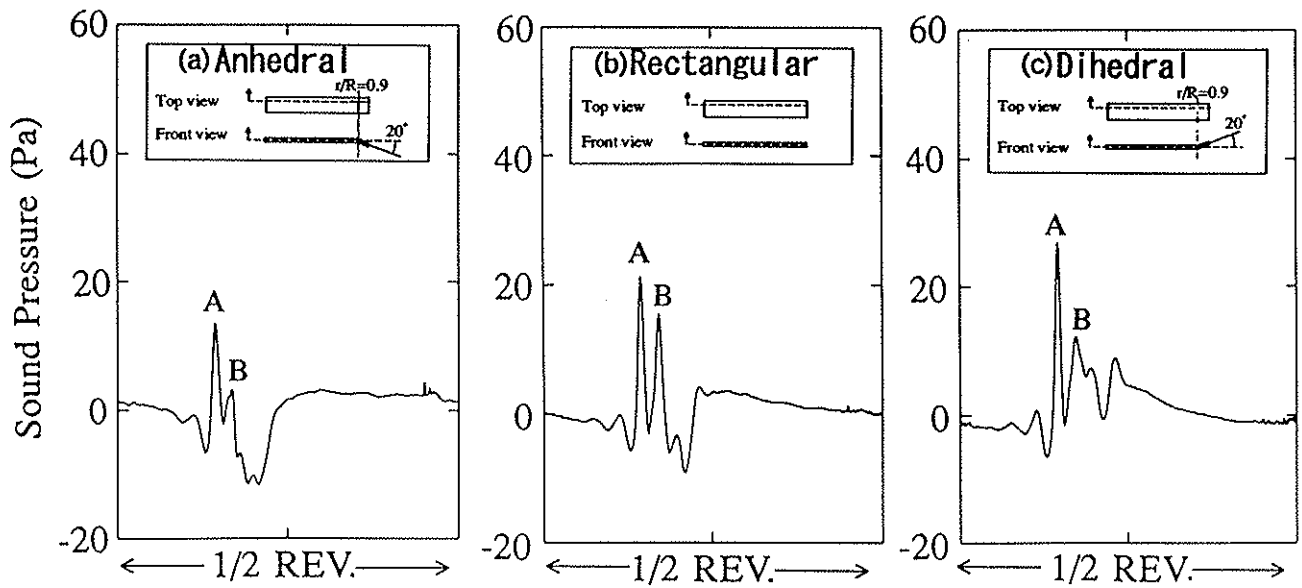


Fig.6 Time histories of BVI noise for blades with anhedral, rectangular, and dihedral tip shapes.

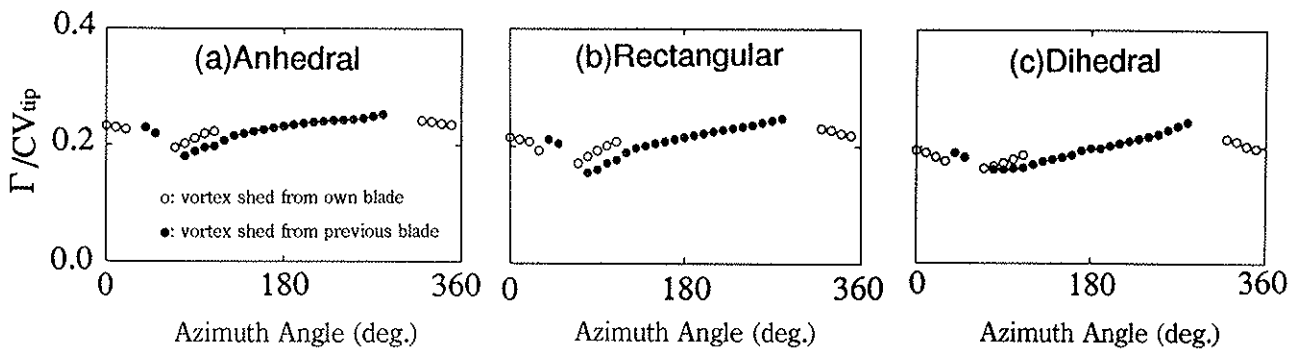


Fig.7 Strength of tip vortex during BVIs for blades with anhedral, rectangular, and dihedral tip shapes.

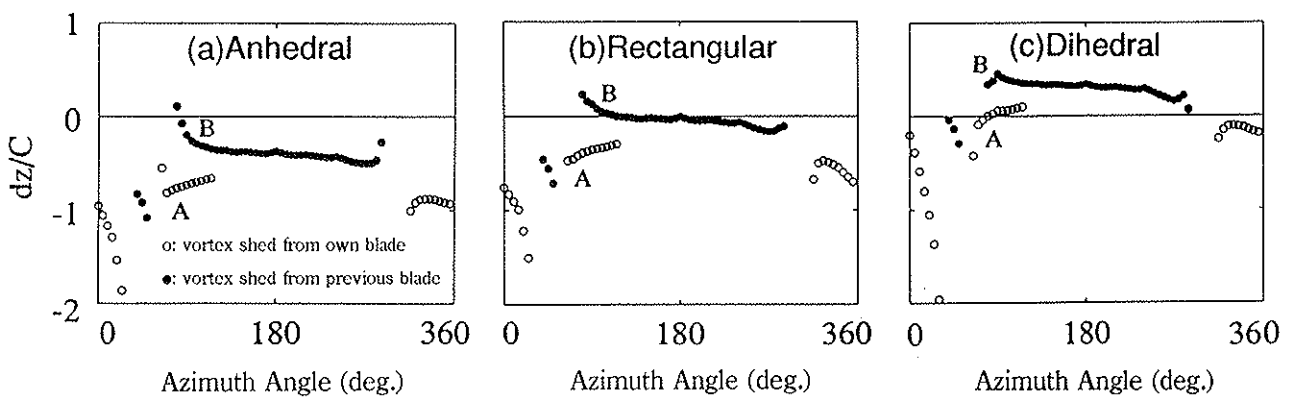


Fig.8 Miss-distance between vortex and blade during BVIs for blades with anhedral, rectangular, and dihedral tip shapes.

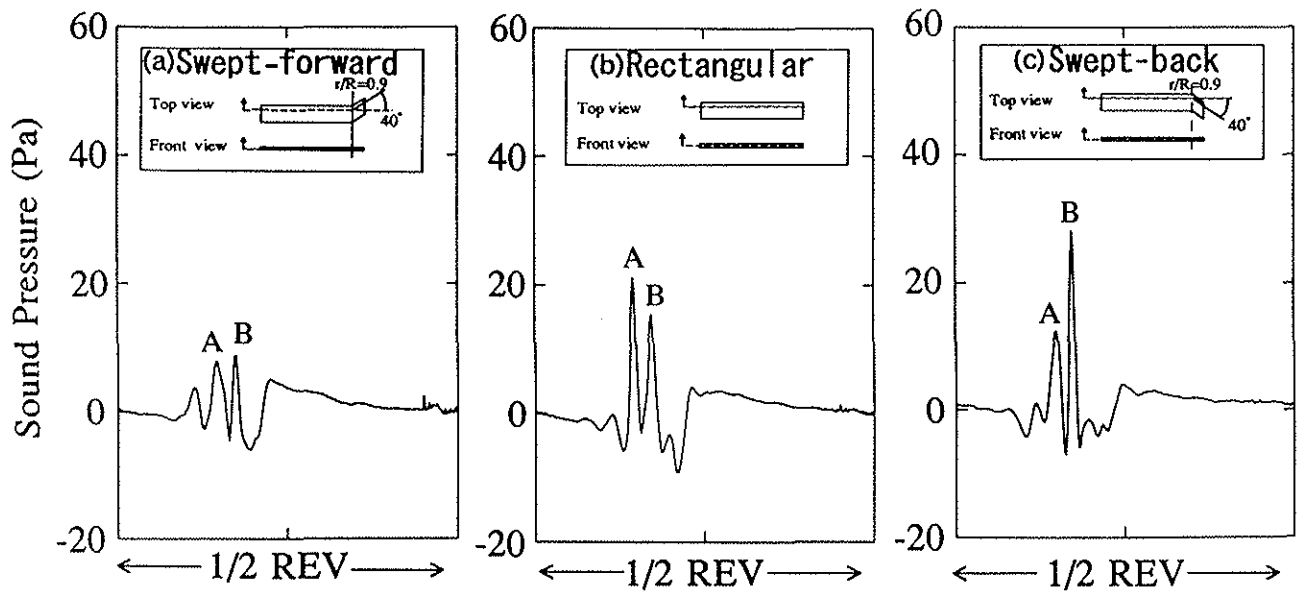


Fig.9 Time histories of BVI noise for blades with swept-forward, rectangular, and swept-back tip shapes.

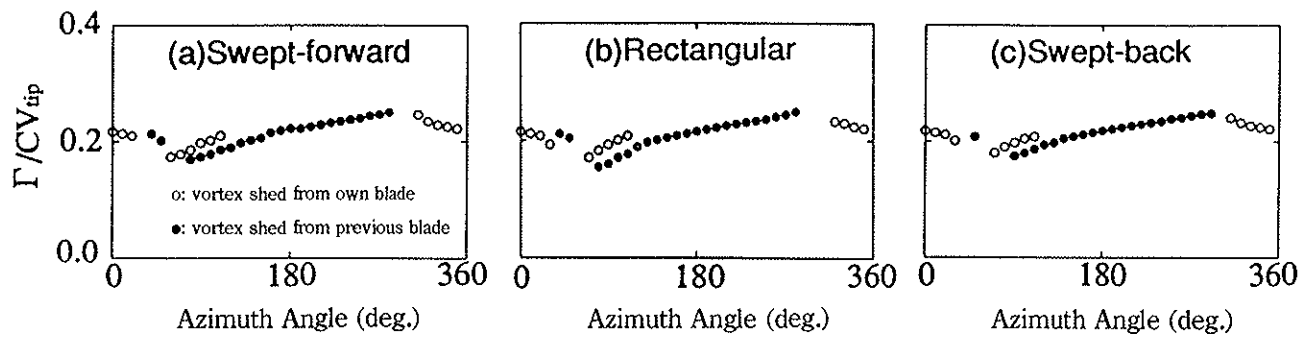


Fig.10 Strength of tip vortex during BVIs for blades with swept-forward, rectangular, and swept-back tip shapes.

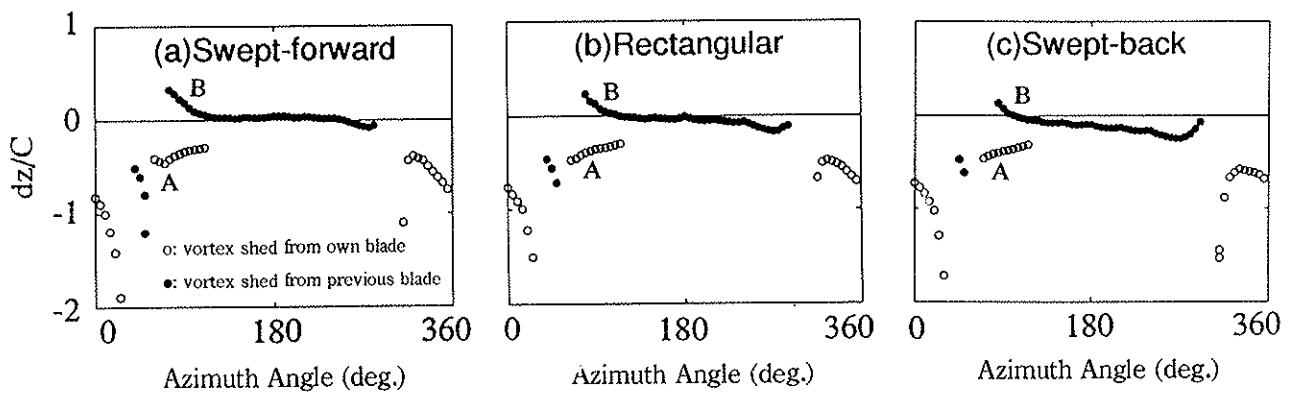


Fig.11 Miss-distance between vortex and blade during BVIs for blades with swept-forward, rectangular, and swept-back tip shapes.

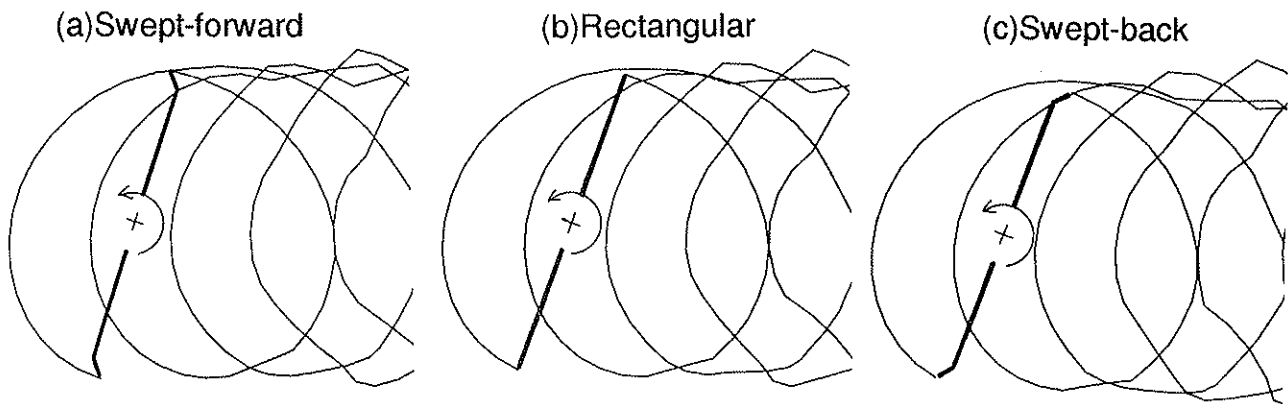


Fig.12 Trajectories of tip vortices for blades with swept-forward, rectangular, and swept-back tip shapes.

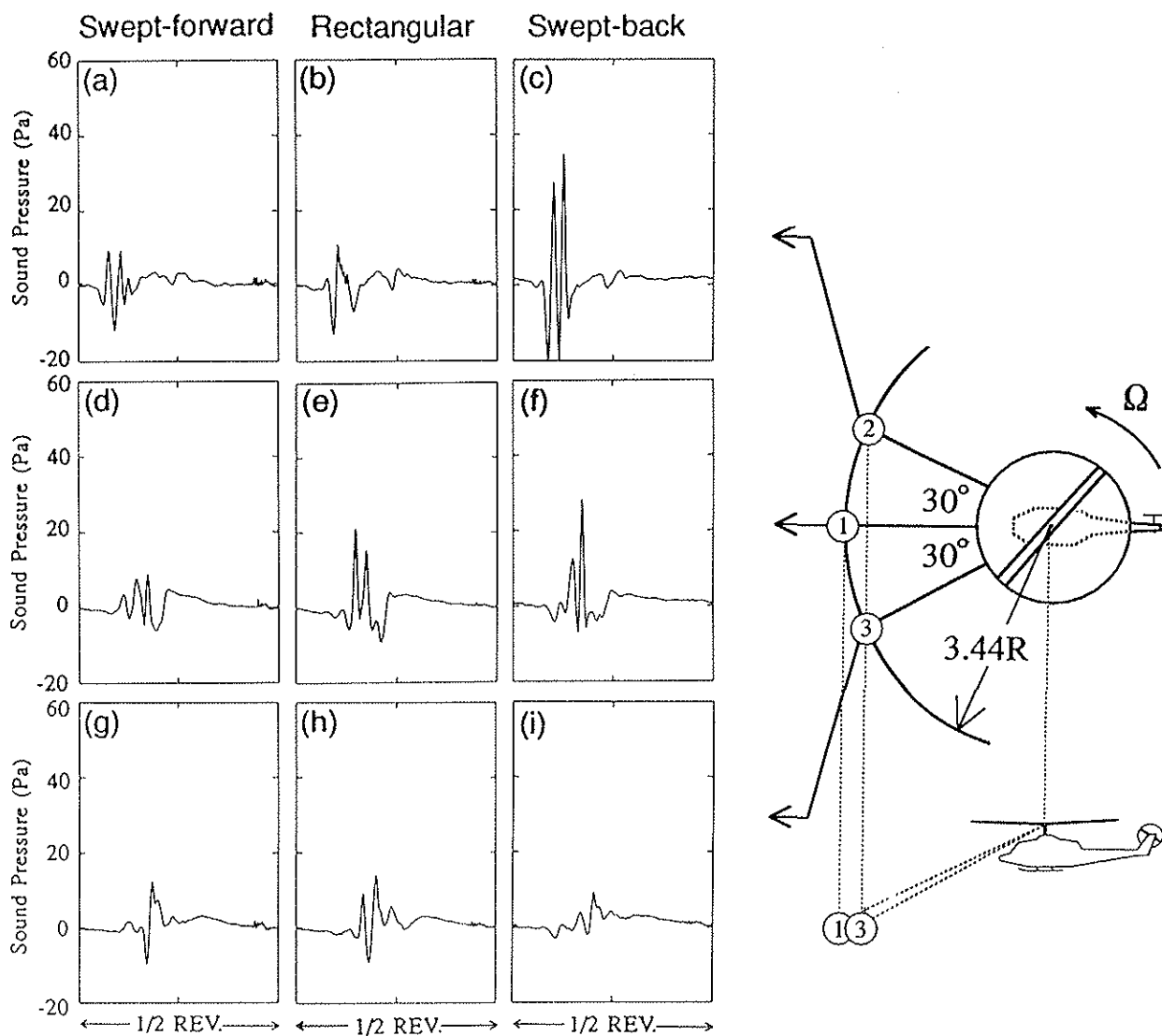


Fig.13 Effect of swept tip shapes on directivity of BVI noise.

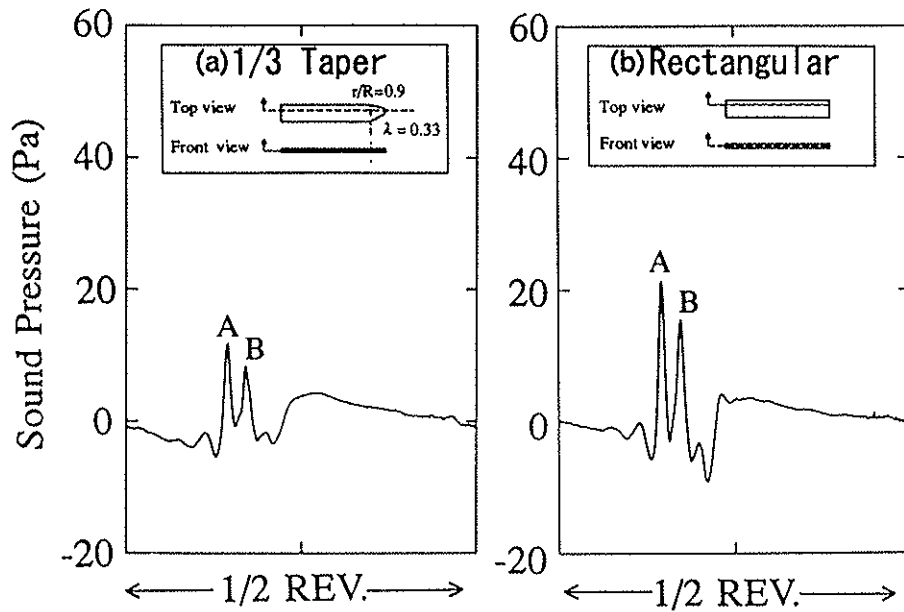


Fig.14 Time histories of BVI noise for blades with tapered and rectangular tip shapes.

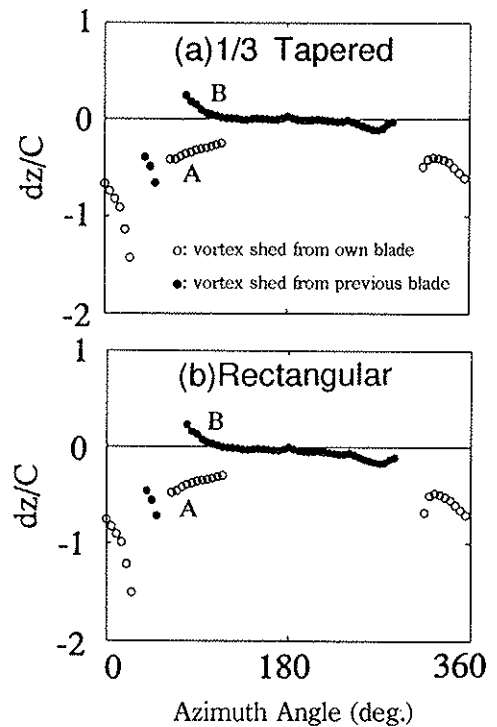
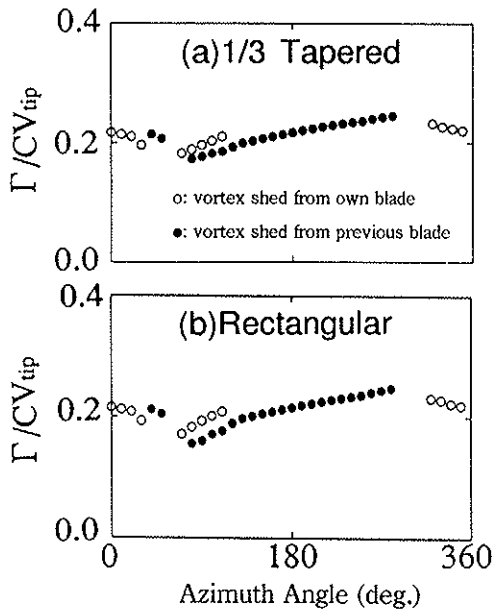


Fig.15 Strength of tip vortex during BVIs for blades with tapered and rectangular tip shapes.

Fig.16 Miss-distance between vortex and blade during BVIs for blades with tapered and rectangular tip shapes.

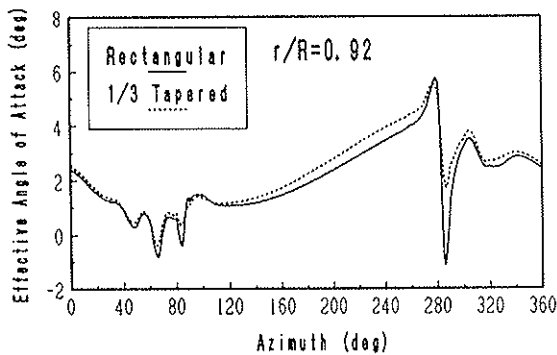


Fig.17 Time histories of effective angle of attack for blades with tapered and rectangular tip shapes.